Design of a Swirl Distortion Grid and CFD Validation

S. De la Asunción Mollá, E. Benichou and V. Maillet
Institut Supérieur de l'Aéronautique et de l'Espace (ISAE-SUPAERO), Université de Toulouse, 31055 Toulouse, FRANCE
Email: salvador.de-la-asuncion-molla@student.isae-supaero.fr
Email: {emmanuel.benichou,vincent.maillet}@isae-supaero.fr

***Abstract*—Swirl distortion is attracting considerable interest due to its implication for new aircraft topologies such as blended wings with integrated engines. This paper proposes guidelines to develop a swirl generator grid using the StreamVane method. Different methodologies regarding the seeding strategy are studied, both in the placement and the spacing of the seeding points. The different grid configurations were subjected to a CFD analysis to determine the generated swirl pattern. The distance from the grid at which this pattern was closest to the target one was also investigated. The results revealed that the standard seeding strategy was optimal and that after 20 radius the swirl pattern continued to oscillate. No significant difference was found between the uniform and variable seeding strategy. The StreamVane method has been proven capable of generating complex swirl patterns and providing a valuable tool for the study of complex inlets.**

I. Background

Engine performance is strongly dependant on the characteristics of the incoming flow, making it essential for engineers to study the possible distortions introduced in the flow by the engine inlet, from the first stages of the project. [1] There are 3 main types of inlet distortion: total temperature distortion, total pressure distortion and swirl distortion. Pressure distortion has been studied and modeled the most; the effect of total temperature distortion was later recognized as an important factor, especially in military applications. Nowadays, with the increase in power and new vehicle types requiring intricate inlets, swirl distortion is becoming increasingly relevant. [2]

There are two well known examples of aircraft designs which failed to take into account the effect of inlet swirl distortion and had to apply moderate to complex changes in their structures or components. These aircraft are the multi-role fighter plane Tornado and the Airbus A300. Regarding the Tornado, a considerable amount of testing in a full scale prototype had been already conducted, all with good reviews, but when the fighter was subjected to more demanding flight conditions such as high angles of attack or supersonic speeds, compatibility problems between the airframe and the engine were observed. The two S-duct inlets (without inlet guiding vanes, IGVs) set bulk swirl in the engine compressor causing it to surge and they had to be redesigned. As for the A300, the inlet that provided air to the Honeywell APU caused a complex swirl in high compressor blade strains, requiring this part to be remodeled to correct the error. After these experiences, swirl generators were developed, capable of creating bulk, 2 rev and 4 rev swirl patterns. [3]

There are several types of swirl distortion but the most common ones are Bulk swirl, which can be co-rotating and contra-rotating, one rev swirl and two rev swirl. When working with the aforementioned inlet types, normally a complex pattern is obtained, as in figure 1, which has simultaneously different types of 'basic' swirl types. The impact of swirl on the compressor depends on its type, for example it is expected a reduction in flow and pressure ratio but an increase in the efficiency and in the stall margin for co-rotating bulk swirl, on the other hand the contra-rotating bulk swirl shows an opposite behaviour. [4]

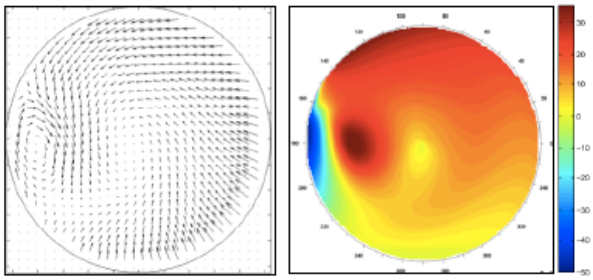

Fig. 1. Complex swirl pattern of a hybrid wing body tested at NASA Langley's wind tunnel

II. Interest

Systems like unmanned aerial vehicles (UAVs), helicopters or auxiliary power units (APUs) require inlets with several flow direction changes. [3] Moreover, civil aviation is under increasing pressure to operate low carbon dioxide emission and silent engines. This has led to the study of new engine – fuselage topologies such as integrated engines which promise to significantly decrease drag, fuel burnt and noise emissions. Furthermore, this configuration takes advantage of the boundary layer ingestion (BLI) concept which can further improve the aircraft efficiency, showing a decrease of more than 16% of fuel spent compared to a conventional configured aircraft. [5] Noise reduction is achieved by the shielding effect of either the wings or fuselage of the engine with respect to the ground.

However, all of these positive aspects come with a drawback, the flow passes through a more complex inlet (normally an S-duct inlet) and as a consequence it get disturbed. The BLI along with other vortices created by the proper fuselage or wings generates strong nonuniformities in the flow, producing swirl distortion among others [5]. It is therefore of great interest for aircraft manufacturers and end - users to understand swirl distortion and come with a cost effective method to reproduced desired patterns.

III. Aim

Swirl generators have been designed both by researchers and private companies in order to test engines at ground level, saving precious time and money in the development phase. Several methods have been proposed; including delta wings, turned vanes and swirl chambers. These methods have proven adequate for generating basic patterns but fail when trying to generate a more complex swirl which can originate from a study of the real inlet either experimentally or frequently via numerical simulations. [1]

A recent thesis by M. Hoopes at Virginia Polytechnic Insitute proposed a new method, called StreamVane Design Method, capable of generating more complex swirl patterns. This approach seeks to create turning vanes perpendicular to the desired flow (expressed as a vector field). The cross-sections of the vanes are such that they produce the desired turning angle at regular intervals along each vane row. Once the grid has been designed, it can be manufactured using a 3D printer and tested experimentally. Two examples of such grids are seen in figure 2. The process in which they are designed makes them extremely adaptable to complex patterns. This research project will try to continue Hoopes' work on the StreamVane Method and its applications. [6]

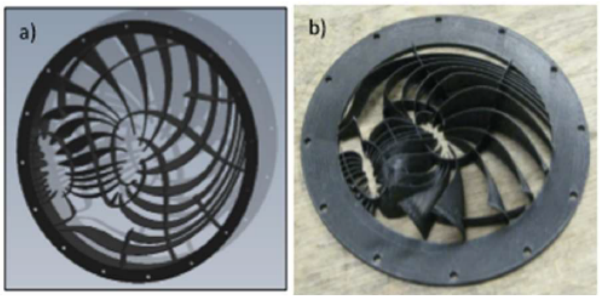

Fig. 2. 3D printed grids designed following the StreamVane Method

The main difficulty that arises when working with this method is the high number of parameters and variables that can be modified by the user. From a single swirl distortion pattern one can obtain completely different turning grids making it difficult to discern the optimal. This project will focus on the effect of varying the seed-line placement and the method to place the seed points along this line, using a target swirl pattern provided by the DAEP department at ISAE-SUPAERO. This pattern can be seen at figure 3.

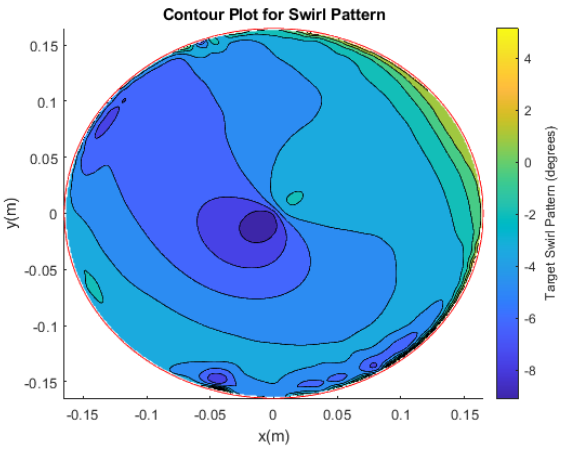

Fig. 3. Target Swirl pattern provided by ISAE - SUPAERO.

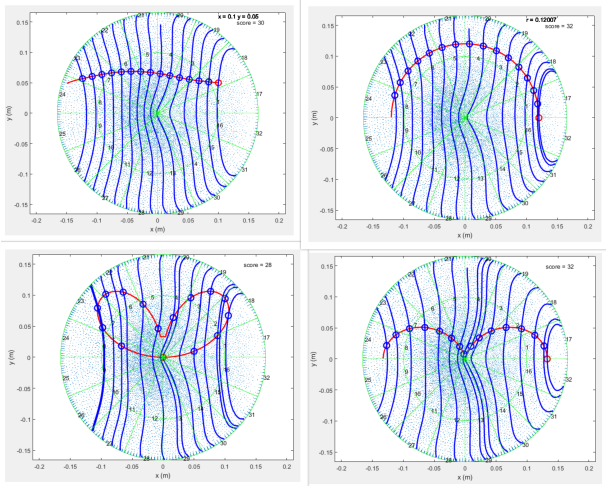

Fig. 4. Different seeding strategies can be seen following the red line. Conventional, semicircle, modified 2 lobes and 2 lobes. In this figures, the red line represents the vane seed line with its start point shown as a red circle. The blue circles represent seed locations for their corresponding vane lines which are also shown in blue.

In the original Matlab code, Hoopes inserted a seed point manually and then computed the streamline following the flow, as ilustrated in the first grid in figure 4. [6] This presents benefits, however it does not adapt to some complex patterns where large parts of the vector field are not reached by the seed-line and therefore no turning effect if produced at those sections. This is especially seen in small-sized, high intensity local vortices at the extremes of the aerodynamical interface plane (AIP). [7] For this reason, new methods to plot this line will be studied such as creating a fixed seed-point line with a pre-determined shape which does not follow the flow.

Furthermore, the method for placing the secondary seed points in this seed-line will be studied. There are two possible options; using a uniform seed spacing which places the seed points at a constant curvilinear distance from each other, and a variable seed spacing that places these points at a constant turning angle from each other.

These new grids will be analysed as well as the original method using the CFD program STAR-CCM+. The output swirl patterns will be compared against the original target pattern in order to obtain the best strategy for creating swirl generator grids.

IV. Methodology

The project was divided into four distinct stages. The first was performed in Matlab, where the target swirl pattern and the parameters were introduced and a set of coordinates describing the grid was obtained as an output. The second stage corresponds to the creation of the 3D grid which was necessary to import it to STARCCM+ and perform the simulations. This creation was performed in the computer aided design (CAD) software CATIA. In the third stage the numerical simulations in STAR-CCM+ were performed and in the last stage the generated swirl distortion patterns were compared using Matlab.

A. Grid design

The first stage was the most time consuming as many parameter changing iterations were needed. The scripts super_seed_path_maker and blade_and_path_maker were used.

The first script input is the target swirl distortion pattern and attending to various parameters, it outputs a 2D schema of vane placement, as seen in figure 4. The seeding strategy is choosen in this script, both in the placement of the seeding line and the type of spacing (uniform or variable). For the seeding line, two shapes were chosen: a semicircle and a 2 lobe form, second and fourth images in figure 4 respectively. These variations were compared with the standard configuration devised by Hoopes where a point is chosen and the seeding line is automatically calculated following a perpendicular direction to the turning angle (first image in figure

4). For the semicircle, both the uniform spacing and the variable spacing were studied. For the 2 lobe shape only the uniform spacing and for the standard seeding line only the variable spacing; making a total of four distinct grid configurations.

In this first script a function that generated a score for each grid was implemented. This score was based on the area covered by the grids, the more area covered the higher the score it received. This was extremelly helpfull because grids could be generated in big batches of 20 to 60 grids, varying one parameter at a time and only the best grid was finally chosen. This can be seen in figure 5, the plane is divided in 32 sectors (seen in green) and at the top right position the score is shown.

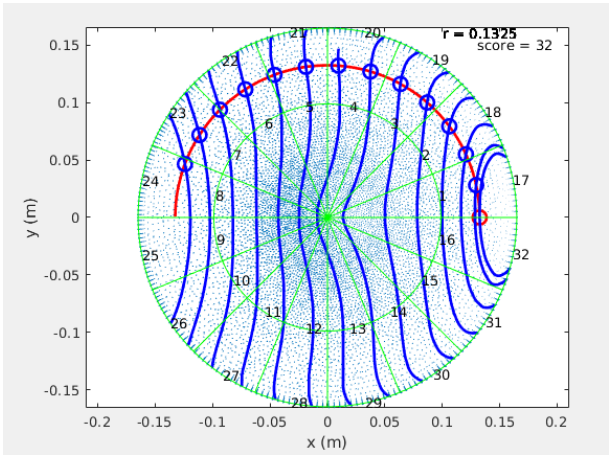

Fig. 5. Score and sector visualization in the 2D representation of the vanes

The second script inputs are the 2D coordinates generated by the super_seed_path_maker script and this creates the 3D representation. In this section the thickness, chord and profile of the vanes are specified. A NACA A4K6 camber line was selected for the profile as it is recommended for inlet guide vanes [6]. A4K6 camber line provides an accurate flow guidance over a large range of output turning angle and is relatively easy to implement. This is corroborated by an extensive experimental investigation performed by Dunavant [8]. A parameter controlling the boundary layer is also relevant in this program; the first script generates thousands of points in the boudary layer and these points need to be removed to obtain a correct 3D object. Finally, a set of csv files is outputed by the script (one per vane). A complementary 2D representation is also offered, showing the final position of the vanes. The 2D sketch generated by the super_seed_path_maker script is similar to the end result but not the same since it can be modified by certain parameters in the blade_and_path_maker script , an example of this is shown in figure 6, representing the final vane placement for the 2 lobe configuration.

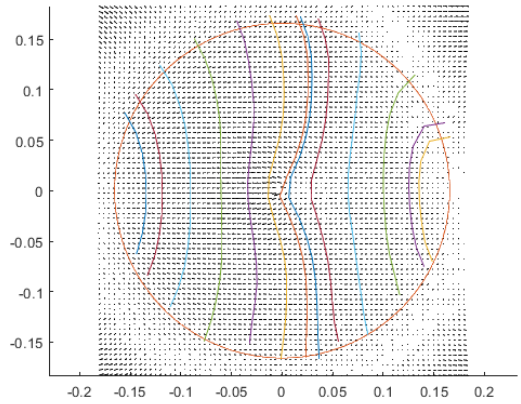

Fig. 6. 2D representation of the output of the blade_and_path_maker script

B. Creation of the 3D grid

Once all of the csv files were created, they were imported to CATIA using a macro. A cleaning process was executed in this program, deleting some vanes that had been created too close for instance. Once the final result was as desired, the 3D objects were exported as STP files. This type of files can be readily imported to STARCCM+ as a surface mesh. An ilustration of the base case using uniform spacing is shown in figure 7.

C. Simulation in STARCCM+

The programm STARCCM+ was chosen to perform the RANS simulation as it is an all-in-one solution for both the meshing and the numerical resolution. The first step was to create a domain for the simulation. It was chosen a cylindrical vane of radius 0.1656 m (equal to the grid radius) and length $10 * Radius$ from the inlet to the grid and $20 * Radius$ from the grid to the outlet. This distances to the inlet and outlet boundaries showed to be enough to achieve a stable flow at both ends.

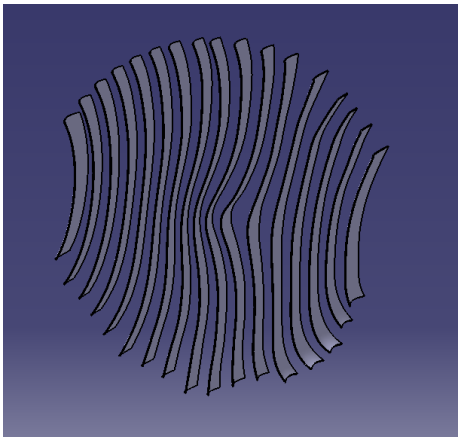

Fig. 7. 3D grid created by CATIA. Base configuration, uniform spacing.

TABLE I
PHYSICS MODELS AND MESH REFERENCE VALUES

Physics Models	Mesh Reference Values	Values
All y+ Wall Treatment	Base Size	0.08 m
Coupled Energy & Flow	Number Prism Layers	20
Gamma-ReTheta Transition	Prism Layer Thickness	2.85 mm
Gas	Prism Layer Stretching	1.2
SST K - Omega	Surface Growth Rate	1.1
Three Dimensional	Main Target Size	4 mm
Turbulent	Grid Target Size	2 mm
Steady		

The next step in the simulation configuration was the physics models setup. A turbulent approach was necessary as the Reynolds number is around 500 000, showing therefore a completly turbulent behaviour. It was chosen a coupled flow solver with the $K-\omega$ SST model and Gamma-ReTheta transition model. This models were chosen following literature advise in adittion to the recomendation of my tutors. The full physics parameters are shown in Table I.

An unstructured mesh was used with the Polyhedral Mesher for the body of the mesh and a Prism Layer Mesher to capture correctly the flow near the walls. A general target size of 4 mm was imposed for the general mesh and then a custom target size of 2 mm was set to the grid boundary to correctly model the behaviour at the grid level, where the flow is disturbed. A relative fine mesh all around the domain was needed as the swirl angle had to be analysed with precision at different planes downwind the grids. The main mesh reference values are shown in table I.

The mesh was configured in the cylindrical surface boundary to resemble as much as possible a cylindrical wind tunnel vane as a coherent follow-up to this project is to perform an experimental study. This curved surface of the cylinder was set to slip condition which means no prism layer is constructed and there is no boundary layer created at this walls.

The inlet boundary was set up as a stagnation inlet with the Total pressure and Total temperature being provided by my tutors after a CFD analysis of the whole body in flight conditions at $Mach = 0.11$ and ground level. The outlet boundary was set to a pressure outlet with a target mass flow rate of 8.09 kg/s , calculated also by the complete CFD analysis provided by my tutors.

The boundary layer thickness was calculated to be 2.55 mm and the first layer of the prism layer measured 0.015 mm to capture correctly the near-wall effects. The target wall y+ was equal to 1 but finally values varied from 1 to 5 (between 1 and 3 in most of the grid), as it is shown in figure 8. This y+ values are sufficiently low as they still capture the behaviour in the viscous sublayer.

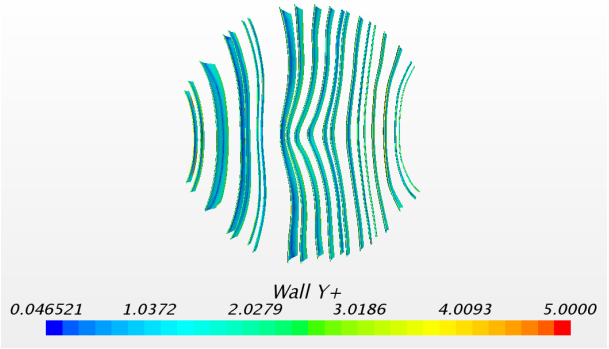

Fig. 8. Wall Y+ representation for the semicircle, variable spacing grid

The resulting number of cells using this parameters was approximatelly 10 million. This number varied between the four different configuration due to slight changes in the grids geometries, the minimum number of cells were 9.2 million and the maximum 10.1 million. A close-up of the mesh can be seen in figure 9.

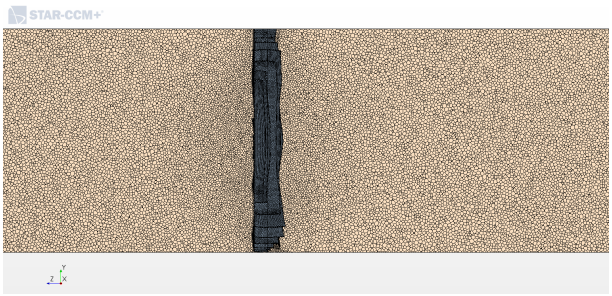

Fig. 9. Mesh representation along X = 0 plane

The simulations were set up with a Courant number of 15 and took approximatelly 5000 iterations to converge. The convergence was confirmed using several monitors: the residuals, the mass flow difference between the inlet and outlet and the pressure calculated in a grid of 16 points at 0.2 m downstream the grid.

A mesh sensitivity analysis was performed using the error and change in the aforementioned monitors (respectively mass flow and pressure grid). A total of 7 iterations in the mesh were generated improving the previous ones until the mass flow error was of the order of 10^{-6} and the pressure difference between the last 2 meshes was of less than 3%.

To extract the swirl pattern at different distances downwind from the grids, ten planes were created at a constant distance of 0.3 m from each other, having the closest one a distance of 0.3 m to the grid and the furthest one 3 m. The planes can be seen at figure 10

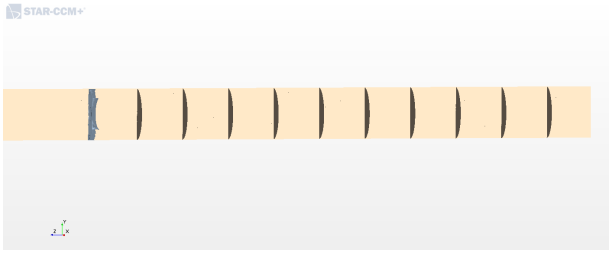

Fig. 10. Planes downwind used to compare the swirl distortion pattern at different distances from the grid

D. Post processing in Matlab

The final step was to compare the swirl pattern extracted at the ten planes for each configuration. Two conclusions wanted to be extracted from this last step: which of the four configurations produced the most similar swirl distortion to the original one and at which plane distance.

The first processing stage was to calculate the swirl error from the velocity components extracyed from the simulations. The following equations were used for this purpose:

$$velocity_{plane} = \frac{\sqrt{(2)}}{2} * (u + v)$$

$$swirl = \arctan(\frac{velocity_{plane}}{w})$$

$$swirl_{error} = swirl_{target} - swirl_{generated}$$

To compute the error, the root mean square error (RMSE) will be used. The RMSE is a frequently used measure of the differences between values predicted by a model and the values observed. The RMSE represents the square root of the second sample moment of the differences between predicted values and observed values. The RMSE serves to aggregate the magnitudes of the errors in predictions for various data points into a single measure of predictive power [9]. The RMSE will be calculated using the automatic Matlab function, which uses:

$$RMSE = \sqrt{E((Swirl_{error})^2)}$$

Three different types of approaches were used to represent the error: a 3D, a 2D and a 1D approach. The 3D approach substracts the original swirl pattern from the recovered pattern and plots it, this way it can be graphically seen the differences between both distortion patterns and where the difference is more prominent. The 2D approach gets the differences in swirl along 3 different circles at 3/4, 1/2 and 1/5 of the grid radius and averages them in each circle, this circles can be seen in the top plot in figure 13. This method is useful to obtain a numerical value (and not just a graphical result as in the 3D approach) capable of discerning where the root mean square error (RMSE) is more prominent; at low radius or high ones. This information can be

used to improve the grids in a future work. Finally, the 1D approach calculates all of the differences in swirl and computes the RMSE to obtain a single number describing the total error all around the plane. This 1D approach is useful to compare between grids and will be the criteria used to finally check which plane and grid configuration is the best one.

V. Results & Discussion

After the convergence of the simulations, several scalar and vectorial quantities were studied to obtain a general idea of the impact of the grids on the flow. Figure 11 presents the velocity profile at the $x = 0$ plane. The velocity upstream is 87.8 m/s. Once the flow passes through the grid it gets accelerated near the outer surface of the domain to a velocity of 91.1 m/s, and as expected the flow decreases in velocity near the axis to a value of 87.1 m/s.

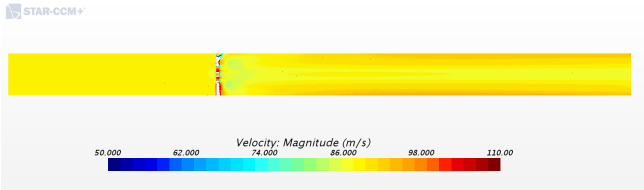

Fig. 11. Velocity scene for the base configuration using variable spacing. Plane x = 0.

To compare the variable and uniform spacing the $z = 0$ plane at the grid level will be used. In figure 12 the transversal cross-section, for both configurations of the semicircle are shown. For the variable spacing strategy (top image), it is observed that the flow is slightly accelerated at the left and decelerated at the right. The reason for this result is still not entirely clear but it can be justified by having the right side a larger number of vanes and therefore less free space for the flow to pass through. The fact that between two close vanes the flow is also highly decelerated strengthens this hypotheses. This is indeed a problem with the variable spacing method, if the turning angle gradient is higher at one point it will try to increase the number of vanes, sometimes excessively. The only way to solve this is during the cleaning process in CATIA. On the uniform spacing strategy (bottom image) the same behaviour is observed with a much higher velocity at the left side, in principle invalidating the previous theory as it has approximately the same number of vanes in both sides. The reason for this is yet to be known.

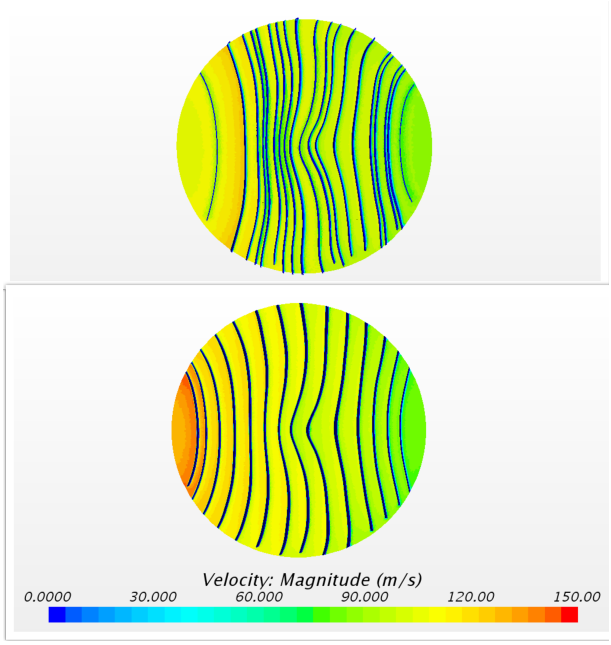

Fig. 12. Velocity scene for the semicircle configuration, plane x = 0. Top image using variable spacing and bottom using uniform spacing.

The swirl RMSE at the best plane (lowest 1D RMSE) for each configuration is presented in table II. It can be observed that the best configuration corresponds to the Base case using variable spacing, closely followed by the 2 lobe uniform spacing configuration. From now on the base variable spacing configuration will be presented.

TABLE II
Summary of Swirl RMS Errors

Configuration	Swirl RMSE [deg]
Base Variable Spacing	2.63
Semicircle Uniform Spacing	3.02
Semicircle Variable Spacing	2.93
2 lobe Uniform Spacing	2.64

It can be observed in figure 13 the quiver and contour plots for x = 3 m. The quiver plot represents the i and j velocity errors in the plane as vectors; it

can also be observed the three different circles that are used to calculate the 2D error (dashed lines). The contour plot is a useful tool to understand graphically the position and magnitudes of the errors. It is seen that the RMSE varies from 0 to 3.5 being especially high in the right of the plane. This high RMSE at the right of the plane is seen in all of the different configurations and planes. A possible explanation for this is that the grids did not cover completely this right part of the plane. Nevertheless the left part was also not covered completly and the error in that side is relatively low.

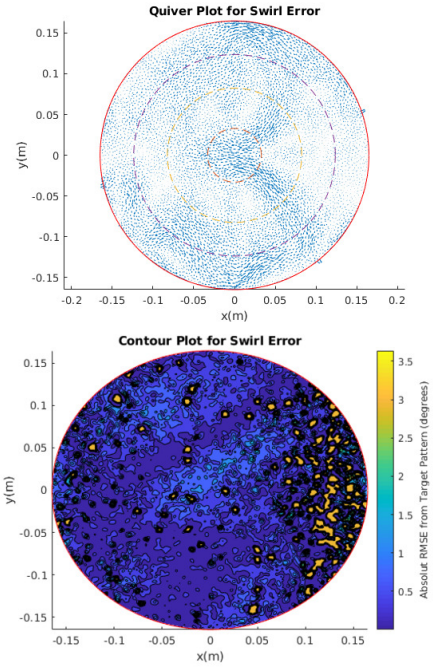

Fig. 13. Quiver and Contour plots for the base configuration, variable spacing, at 3m

In order to examine the plane distance effect, a graph showing the RMSE for each configuration against distance is seen in figure 14. As aforementioned, the best configuration is the base case, but all of the configurations show a similar behaviour. It is noted that all of the cases (except the 2 lobe) show a slight decrease during the first 5 radius and then start oscillating around its mean RMSE value. The correlation between the distance and RMSE is not evident. Once the results were seen, it would have been better to make a longer domain to see if the flow stabilizes at higher radius.

The results at figure 14 show there is no clear

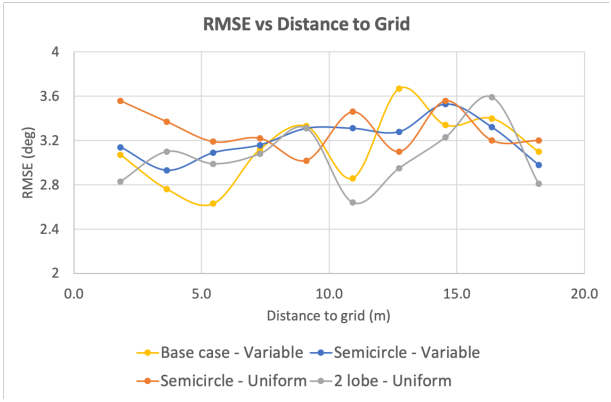

Fig. 14. Swirl RMSE against Plane Distance

difference between using a predetermined shape and the base method. No significant change in the RMSE is seen between the different shapes tested nor between the uniform and variable spacing in the semicircle configuration; although the variable spacing grid had a 3% lower error. Both the magnitude and the layout of the error is similar in all of the configurations, as seen in figure 15. It can be observed that all of the different grids generate a very similar 3D RMSE.

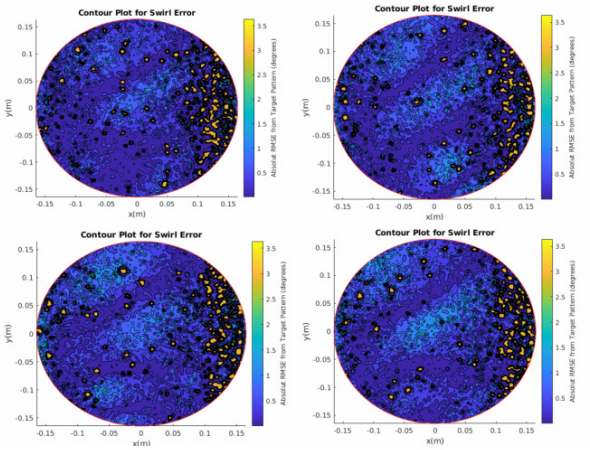

Fig. 15. Contours showing the RMSE for: Base case, Semicircle - Variable, Semicircle - Uniform and 2 Lobes

There are several possible explanations for deviations between the target swirl distortion pattern and the obtained. The target pattern was obtained from a CFD analysis in an open fluid whereas the present study was done using a wind tunnel approach. This may be the explanation of the errors near the boundaries, as seen at the bottom of the contour plot

in figure 13. The CFD mesh was all the fine it could be with the available resources, it is expected that with a finer mesh (especially in the main body) more accurate results would be obtained. The StreamVane Method also makes certain assumptions to simplify the design, such as the linearity of turning angle between vanes. Along with this, there are regions in the grid plane without vanes, meaning no turning of the flow is done. This last reason is the possible source of error seen at the right of the plane. [6] Lastly, to create the contour plot, some data had to be interpolated to obtain the required mesh grid. The interpolation can cause some difference between the actual CFD simulation and the post-processed plot.

The results obtained were slightly disappointing as the error was relatively big. Nevertheless, these values are approximately close to the ones seen at the literature, the RMSE obtained by Hoopes is of approximately 1.6 deg and whilst it was calculated using a very simple swirl patterns generated by Matlab, they are just 50% smaller than the ones generate in this study. This results show that the StreamVane Method is useful when working with complex swirl patterns and not just bulk or 2 rev swirl patterns.

VI. Conclusion and Future work

This study focused on investigating and trying to improve the StreamVane Method by adding some functionalities regarding the seeding process. Furthermore it was examined the usefulness of this method when dealing with real life swirl distortion patterns. The main purpose remained adquiring skill of the StreamVane Method for its future use as a standard step in aircraft design.

During this project, it was shown that the best configuration was the base case using variable spacing but very close to the 2 lobe configuration. All of the grids tested performed in a similar way. No significant difference was observed between both spacing methods. It was intended to test a grid using the base case and uniform spacing but due to computational issues and lack of time it had to be discarded. All things considered, the post processing in CATIA showed more important than the spacing method, having to make some final changes like deleting duplicate vanes created by the variable spacing method.

The information on the flow distance stabilization is also an interesting outcome of this project. The evidence from this study suggests that after the 20 radius that were available the swirl patterns had not still converged so a longer domain should be studied. In addition to this, the correlation between swirl RMSE and distance seems to be practically identical between different configurations of grids, making it easy for future work to reach an optimum stabilization distance. These findings add to our understanding of swirl distortion generators.

A more extensive CFD study could be performed, using more shapes and different swirl patterns with the presence of local vortices. The studied pattern lacked local strong vortices so it could not be proven the efficacity of the grids when facing these complicated patterns. More complex swirls will maybe require two different seeding lines to correctly capture all of the plane, this could also not be tested using the current swirl pattern.

Another coherent follow-up to this project is an experimental study to corroborate the CFD results. As the final aim of the swirl generating vanes is to detect incompatibilities between inlets and engines experimentally, the wind tunnel study is of key importance.

On a broader level, research is needed to determine if the changes in pressure resulting from this type of experiments, where a grid that clearly disturbs the flow is used, creates pressure distortions. As this type of inlet distortion are imporant for inlet - engine incompatibilities.

Acknowledgment

I would like to thank my tutors E. Benichou and V. Maillet for their help all along the project; the useful advice they gave me and the results from their CFD simulations showed crucial for the development of the project. I also really appreciate the resources put at my disposal by ISAE SUPAERO and especially the DAEP department without which I could not have carried out this research project.

References

[1] T. Guimarães, "An overview of recent results using the streamvane method for generating tailored swirl distortion in jet engine research," *AIAA*, 2016.

[2] J. Yao, "A time-accurate cfd analysis of inlet distortion induced swirl in multistage fans," *AIAA*, 2007.

[3] Y. Sheoran, “A versatile design of a controlled swirl distortion generator for testing gas turbine engines,” *ASME*, 2008.
[4] Y. Sheoran, “Compressor performance and operability in swirl distortion,” *ASME*, 2012.
[5] D. J. Frohnapfel, “Experimental quantification of fan rotor effects on inlet swirl using swirl distortion descriptors,” *ASME*, 2018.
[6] K. M.Hoopes, *A New Method for Generating Swirl Inlet Distortionfor Jet Engine Research*. Master thesis, Virginia Polytechnic Institute and State University, May 2013.
[7] D. D. Sanders, “Cfd performance predictions of a serpentine diffuser configuration in an annular cascade facility,” *AIAA*, 2013.
[8] J. Dunavant, “Cascade investigation of a related series of 6 percent thick guide-vane profiles and design charts,” *NACA*, 1957.
[9] Hyndman, “Another look at measures of forecast accuracy,” *International Journal of Forecasting*, 2006.